AL-ZAHRAA UNIVERSITY JOURNAL
Health and Medical Science

Al-Zahraa Journal for Health and Medical Sciences 2025; 3:91-104 Vol. 3, No.2, 2025
www.zjhms.alzahraa.edu.iq

Microwave-Assisted Green Synthesis of SBA-15 and its Application on Photodecolorization of Eosin Yellow Dye

Rawaa A. Alattar[1]

[1] Department of Chemistry, College of Science, University of Kerbala, Karbala, Iraq.
* rawaa.a@uokerbala.edu.iq

Received: 19 June 2025, Accepted: 28 June. 2025. Published: 30 June. 2025

ABSTRACT

Santa Barbara Amorphous-15 (SBA-15) was synthesized by the microwave process with triblock polymer pluronic P123 ($EO_{20}PO_{70}EO_{20}$) as the structure-direction agent and tetraethyl orthosilicate (TEOS) as the source of silica. Different approaches were used to characterize the SBA-15 such as Fourier transform infrared (FTIR) spectroscopy, X-ray diffraction (XRD), FESM-EDX, high resolution transmission electron microscopy (HRTEM), thermal gravimetric analysis (TGA) and nitrogen adsorption–desorption (BET) surface area analysis. In this work, we prepared SBA-15 at 100 ^{o}C for 20 min. As demonstrated by nitrogen adsorption-desorption, SBA-15 is a mesoporous material with a surface area, pore volume, and pore size (width) of 392.96 m^2/g, 1.4493 nm and 9.285 cm^3/g, respectively. The optimum conditions for Photodecolorization of Eosin yellow dye by (onto) the SBA-15 surface are, a temperature of 25 °C, an adsorbent dosage of 0.05 g, a dye concentration of 5 mg/L, and a contact period of 30 minutes. It was concluded that pseudo-First order kinetic models were the best appropriate for describing experimental data. Furthermore, the thermodynamic function (ΔH#, ΔS#, and ΔG#) for the active case in the photoreaction was calculated. Revealed that photoreaction proceeded exothermically but was non-spontaneous, as evidenced by a positive Gibbs Free Energy change and a negative enthalpy change.

Keywords: SBA-15, Eosin yellow dye, treatment, Photodecolorization.

Introduction

Santa Barbara Amorphous-15 (SBA-15), a mesoporous material derived from silica, with cylindrical, hexagon-shaped pores[1]. The SBA-15 mesoporous silica sieve features a limited pore size dispersion and adjustable pore sizes between 5 and 15 nm[2]. SBA-15's huge surface area (about 300–900 $m^2 \bullet g^{-1}$), great mechanical and thermal stability, inertness, and environmental friendliness are some of its noteworthy features. One substance that can be used in a number of applications is SBA-15[3]. SBA-15 is usually produced using a cooperative self-assembly process in an acidic environment using the triblock copolymer pluronic 123 ($EO_{20}PO_{70}EO_{20}$) as a template, with tetraethoxysilane (TEOS) acting as the source of silica[4]. SBA-15 is an essential mesoporous material with a highly organized hexagonal structure and big, regulated pores[5]. SBA-15's enormous pore size and volume allow it to be used as an adsorbent[6]. The triblock polymer pluronic P123 ($EO_{20}PO_{70}EO_{20}$), HCl, tetraethyl orthosilicate (TEOS), and H_2O are the raw ingredients used to manufacture the SBA-15 using the microwave process[7]. To reduce energy consumption, SBA-15 synthesis uses microwave technology as an alternative heat source. Rapid nucleation during crystallization can be facilitated by surfactants and silicon species interacting more effectively thanks to microwave synthesis's quick heating, homogeneity, and superior penetration[8]. Consequently, this method could produce uniformly small particles, significantly reduce energy consumption, and quicken the crystallization process[9]. Microwave techniques have been employed recently in earlier studies documenting the manufacturing of SBA-15[10]. The objective of this study is to synthesize SBA-15 using TEOS as a source of silica via the microwave technique in large surface area and then applied in the Photo-decolorization of Eosin yellow dye. The optimal parameters for photoreaction process such as initial pH of dye solution, SBA-15 dose, and temperature, were estimated. Thermodynamic parameters for the photo-decolorization process could be established.

EXPERIMENTAL

Chemical materials

Pluronic P-123 (Aldrich) was used as a template, and tetraethyl orthosilicate (TEOS: 98%, Fluka) as a source of silica. Absolute ethanol (Fluka, > 99%), acetone (Romal, > 99.7%), hydrochloric acid (Fluka, > 98%) and Eosin yellow dye ($C_2OH_6Br_4Na_2O_5$, BDH). All chemicals were used without further purification.

Synthesis of SBA-15

The SBA-15 molecular sieve was made using the microwave method. The triblock polymer pluronic P123 ($EO_{20}PO_{70}EO_{20}$) was the structure-direction agent, while the silica was derived from tetraethyl orthosilicate (TEOS). Six grams of P123 triblock copolymer were dissolved in 140 milliliters of 2 M HCl and forty-five milliliters of deionized water to start the usual synthesis process. The solution was heated to 35°C and rapidly stirred for 20 hours before 12.75 g of TEOS was added. After 20 minutes of microwave heating at 100 °C, it was aged for 24 hours, filtered, cleaned with distilled water, and allowed to dry for 12 hours at 25 °C. After a six-hour calcination at 550 degrees Celsius, the surfactant was removed, yielding a white powder called SBA-15. Using the microwave approach, the processes to produce SBA-15 are shown in Fig. 1.

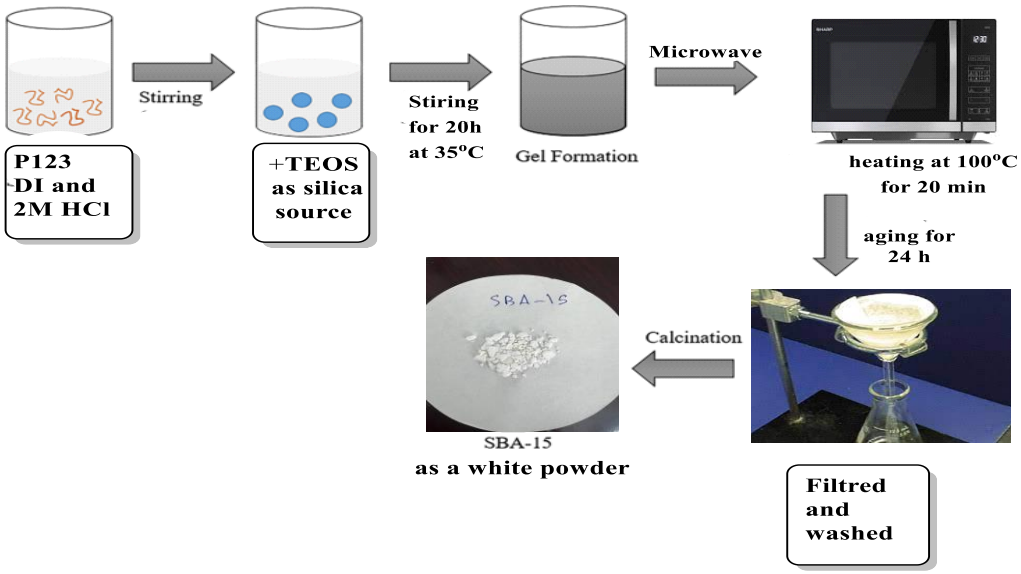

Fig.1 Schematic diagram of SBA-15 synthesis via microwave technique.

Sample Characterization

Using specimens ground into KBr and pressed into discs, FT-IR spectra were captured on a Shimadzu 8400 spectrophotometer in the 4000–400 cm^{-1} range. A Shimadzu X-ray diffractometer was used to record the X-ray diffraction (XRD) patterns, whilst a BET BELSORP MINI II apparatus was used to perform the nitrogen adsorption/desorption analysis. Thermogravimetric analysis (TGA/DTA) was performed on an SDT Q600 V20.9 Build 20 and high-resolution transmission electron microscopy (HRTEM) to 20 nm.

RESULTS AND DISUSSION

FTIR Spectroscopy Analysis

The FT-IR spectrum of SBA-15 is presented in Fig. 2. The hydroxyl bond stretching vibration of silanol (Si-OH) groups and the remaining absorbed water molecules are responsible for the broad band seen at 3410 cm^{-1}. At 1643 cm^{-1}, the bending vibration of the water's O-H is visible[4]. Si–O–Si asymmetric bending vibrations are responsible for the larger band at 1087 cm^{-1}, while the symmetric stretching mode of the same bond is visible at 802 cm^{-1}[11]. Additionally, the Si–OH bending mode may be associated with the band at roughly 960 cm^{-1}, but the Si-O bond rocking vibration is seen at 470 cm^{-1}. Furthermore, the purely surface modification materials have a peak at 428 cm^{-1} which is associated with the Si–O–Si matrix composite. Moreover, the Si–O–Si matrix composite is linked to a peak at 428 cm^{-1} in the materials that have just undergone surface alteration.

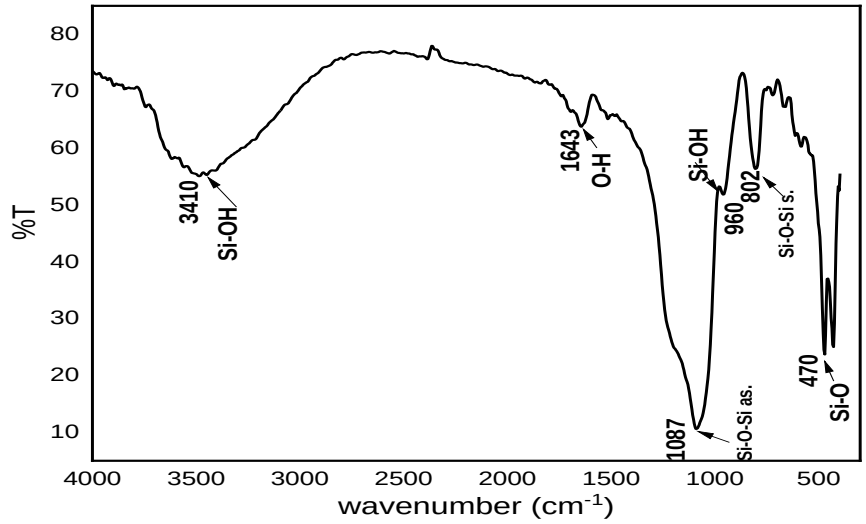

Fig. 2 The FT-IR spectrum of SBA-15.

X-ray Diffraction Pattern

The prepared sample's crystalline nature was examined using XRD analysis, as shown in Fig. 3. The low angle XRD patterns of SBA-15 are displayed in Fig. 3(a). These patterns include three unusual peaks that are linked to the (100), (110), and (200) planes at 2θ angles of 1.96°, 3.45°, and 4.30°. These peaks are thought to be unique to the SBA-15 material.[12] . The high-angle XRD patterns of SBA-15 are displayed in Figure 3(b), which includes a broad typical peak at a 2θ angle

of 10^{o}–20^{o} [13], as well as two peaks to (110) and (200) at 22.65^{o} and 44.02^{o}, and one peak connected to the high intensity (100) plane at 11.8^{o}. A highly organized hexagonal mesoporous silica framework [14], [15], and a two-dimensional (2D) hexagonal mesostructure are correlated with the aforementioned.

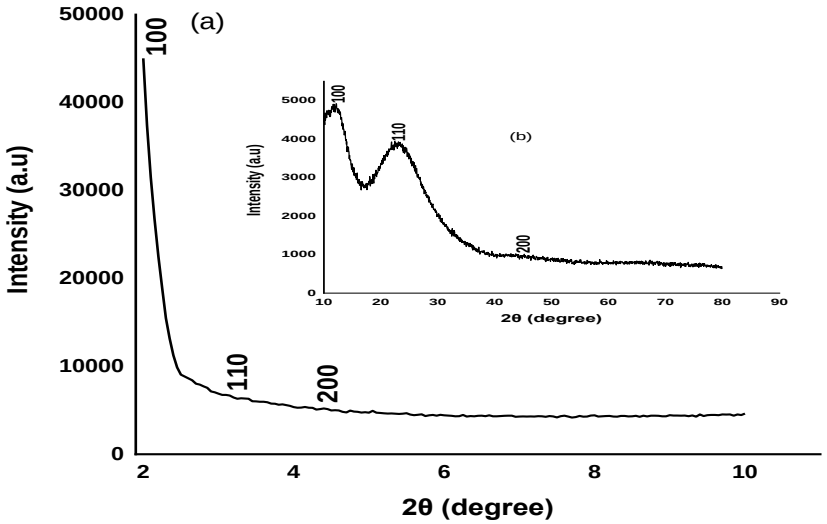

Fig.3 (a) The low angle XRD spectrum of SBA-15 and (b) The high angle XRD spectrum of SBA-15.

N_2- Adsorption-Desorption Analysis

Figure 4 shows the nitrogen adsorption/desorption isotherm curves that were acquired for SBA-15 nanoparticles. The usual type-IV curves found in mesoporous materials were displayed by the SBA-15[13]. A narrow pore size distribution is indicated by hysteresis loops with strong adsorption and desorption branches, which resemble type IV isotherms and type H1 hysteresis loops. BET (Brunauer–Emmett–Teller) and BJH (Barrett–Joyner–Halenda) calculations show that the pore size (width), pore volume, and surface area are, respectively, 9.285 nm, 1.4493 cm^3/g, and 392.96 m^2/g. The mesoporous area is where the pore size distribution of SBA-15 (5–20 nm) is found[16][17]. The SBA-15's notable surface area reductions are a result of employing the microwave technique to shorten exposure times . Temperature tuning can be used to regulate the surface characteristics of SBA-15 during the microwave-assisted synthesis [18].

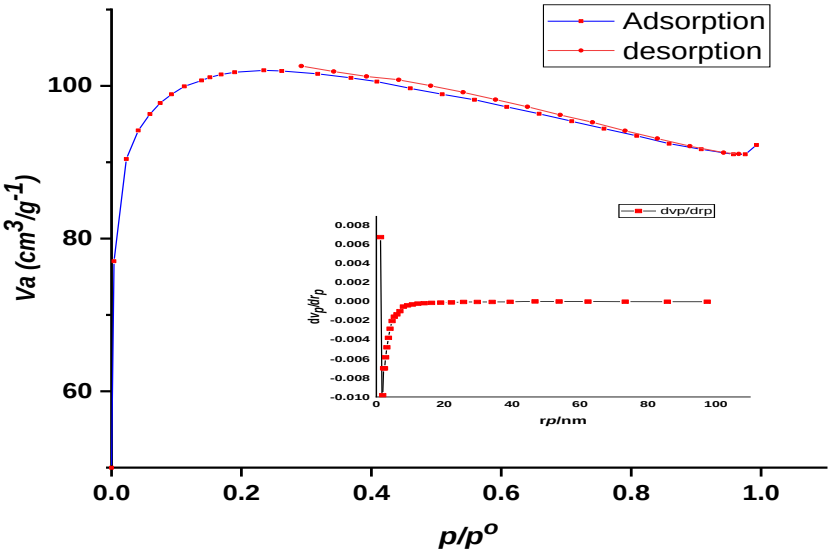

Fig. 4 The N_2 adsorption-desorption isotherm and pore size distribution of SBA-15.

Thermal Analysis - Thermogravimetric Analysis (TGA/DTG)

Figure 5 plots the weight loss of the SBA-15 using TGA analysis [6]. A two-stage mass manufacturing at roughly 25–1000 °C was shown by the TGA result, that is agreement with results in reference[17].

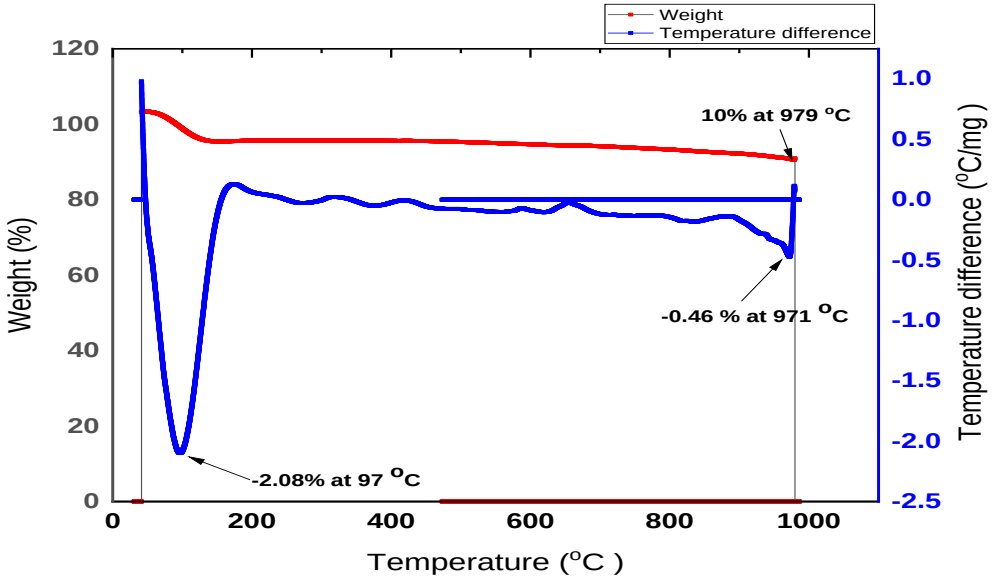

Fig. 5 The TGA/DTA spectrum of SBA-15.

The first step was to remove any water that had been adsorbed onto the silica surface by physical or chemical methods. The Si–OH group in the silica structure was broken down to produce the Si–O–Si siloxane group in the second stage[19]. The thermal gravimetric curve for pure SBA-15 showed that at 978 ^{o}C. The calcined SBA-15 demonstrates both the surfactant's complete removal the impurities during synthesis through the calcination route and the heat stability of SBA-15[7].

TEM analysis

TEM images (Figure 6) of calcined SBA-15 display regular hexagonal collections of mesopores (1D channels) [20]. In addition to confirming that SBA-15 possesses a two-dimensional hexagonal structure .The wall width was expected to be around 9.7 nm using the TEM images [5]. The distance between mesopores is judged to be in agreement with that found from the XRD data based on the high-dark contrast in the TEM picture of this sample (Fig. 6b) .

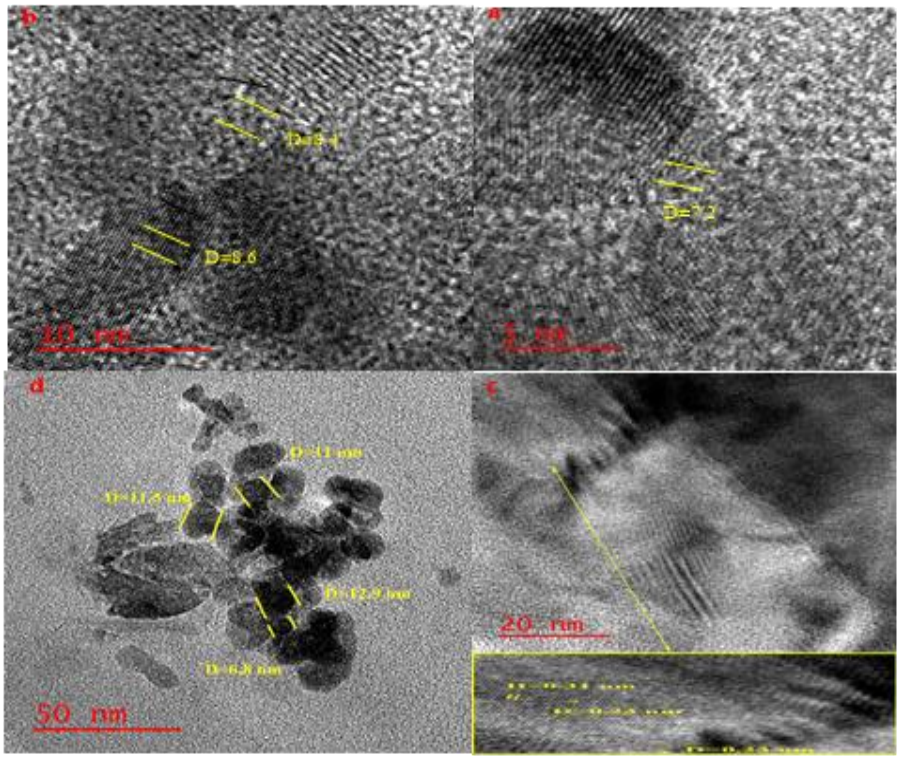

Fig. 6 TEM imagery of (a) SBA-15 on a scale of 5 nm, (b) SBA-15 on a scale of 10 nm, (c) SBA-15 on a scale of 20 nm, and (d) SBA-15 on a scale of 50 nm.

Photodecolorization of Eosin Yellow Dye using SBA-15 as a Surface.

Using a homemade photoreactor, numerous tests were conducted to determine the ideal conditions for photo reactions. The reactor's body is prepared from a wooden box to avoid dangerous light,

which contains an inside 125-watt mercury lamp (UV-A), Pyrex glass beaker (500 mL), magnetic stirrer, Teflon bar, and fun. The light basis of this reactor was parallel set overhead the solution in a beaker flask. The following formulas were used to conclude the photodecolorization efficiency (E_{decol}%) and the apparent rate constant (kapp.) from the photoreaction:[10][21].

$$ln\left[\frac{C_o}{C_t}\right] = K_{app}\,.\,t \qquad (1)$$

$$\%E_{decol.} = \left[\frac{C_o - C_t}{C_o}\right] \times 100 \qquad (2)$$

whereas: C_o and C_t are an initial concentration of dye in dark reaction and a concentration of the same dye at t time of irradiation.

Kinetic of photoreaction

The solution was prepared by adding a suitable weight (0.05g) of studied photocatalysts to 5 ppm of Eosin yellow dye solution. The resulting suspension solution was stirred for 30 minutes to establish an equilibrium state. The UV light was applied on the suspension after the initial step (adsorption). About 3 mL of solution were collected at series intervals time (10- 80 min). The produced filters were twice times separated by a centrifuge, and the absorption of the produced filters was measured at λ_{max} = 510 nm. Using UV-visible spectroscopy[22]. The rate of reaction follows pseudo first-order kinetics, as per the Langmuir-Hinshelwood (L-H) model [23] as shown in Fig.7.

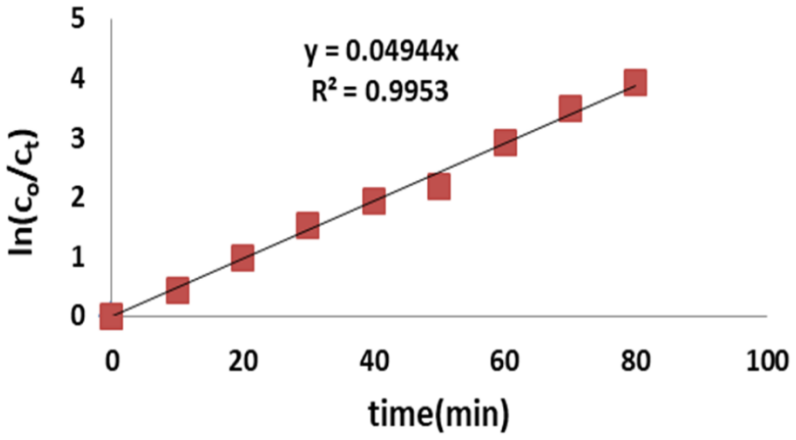

Fig.7: First-order for photo-decolorization of Eosin yellow dye on the surface of SBA-15.

Effect of SBA-15 dose on photodecolorization of Eosin Y. dye.

The effect of SBA-15 doses in the various weights (0.05, 0.10, 0.20, and 0.30 g) is depicted in Fig.8. It was discovered that using 0.05 g of SBA-15 decolorization efficiency reduced from 90.71% to 85% as SBA-15 dosage increased to 0.3 g. According to these findings, lowering the dosage of SBA-15 also reduces the quantity of active sites on the photocatalyst surface, which are necessary for the adsorption process[24].

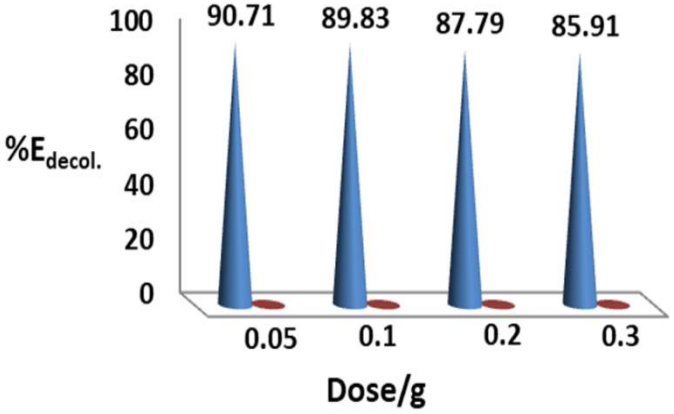

Fig.8: $\%E_{decol}$ of Eosin yellow dye as a function of SBA-15 dose.

Effect of Initial pH of Eosin yellow dye Solution.

Figure 9 shows that when the pH rises from 3 to 9, the proportion of decolorization increases. Two factors could be responsible for these outcomes: the dye's characteristics and the photocatalyst surface's characteristics[3]. Maximum decolorization efficiency is greater than 92.10% at pH 9. Decolorization efficiency in the acidic medium was low.

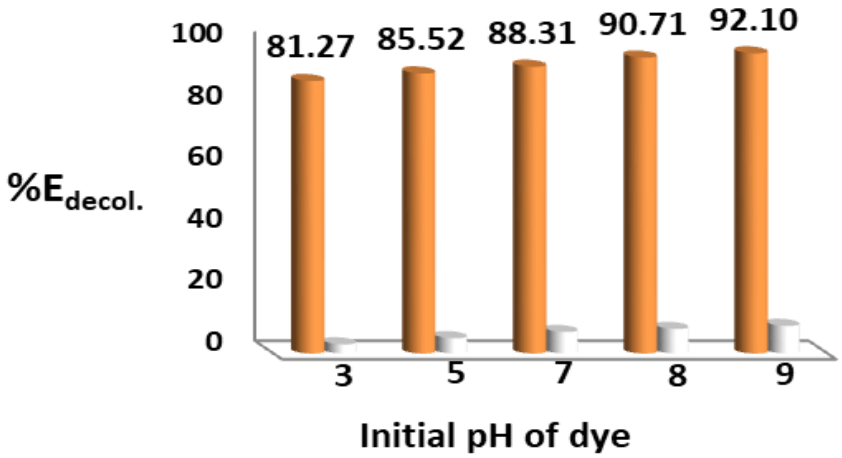

Fig.9: $\%E_{decol}$ of Eosin yellow dye by SBA-15 at different initial pH.

Influencing the temperature on photo-decolorization of dye

In UV radiation and various temperature (10, 15, 20 and 25 ^{o}C), the photo-decolorization percentage of dye (5mg/L) by 0.05 g SBA-15 surfaces at pH=9 was demonstrated in Fig.10, the maximum decolorization proportion was 90.71% at temperature 25^{o}C after 30 min illumination[25]. The Arrhenius equation, the Eyring-Polanyi equation, and the Gibbs equation were used to measure the activation energy (Ea)[26] and thermodynamic function for the active case in photo process (ΔH#, ΔS#, and ΔG#) from the effect temperature range (10-25) ^{o}C.[8]. These consequences are shown in Fig.11(a,b) and table 1.

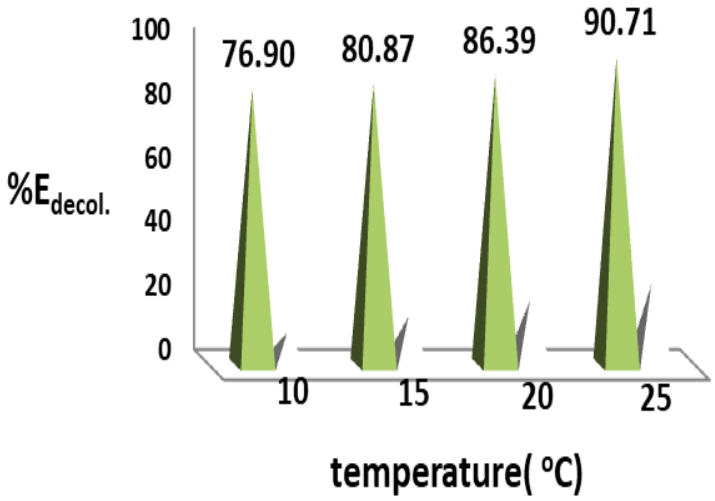

Fig.10: $\%E_{decol}$ of Eosin yellow dye at different temperature.

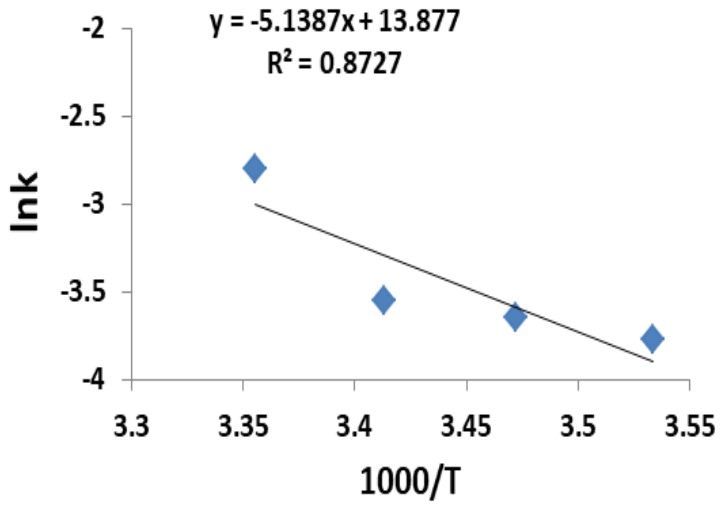

Fig.11(a): Arrhenius eq. design for photo-decolorization of Eosin Y dye at changed temperature.

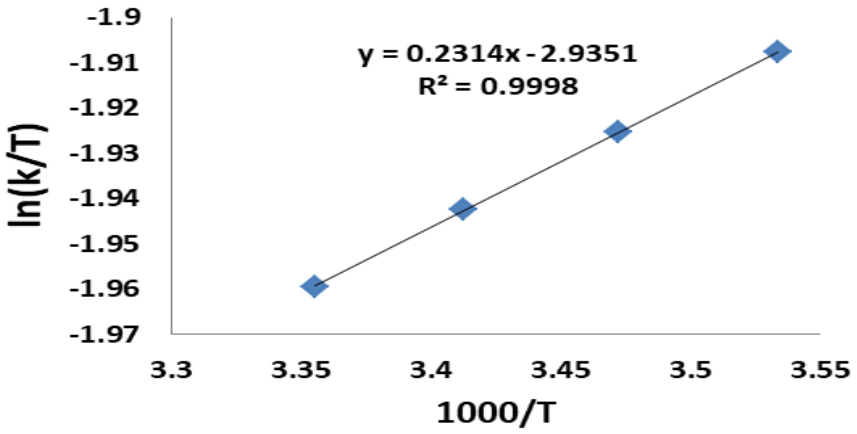

Fig.11(b): Eyring eq. plot for photodecolorization of Eosin Y. dye at changed temperature.

Table 1: Thermodynamic functions and activation energy values of the parameters for the photodecolorization of eosin yellow dye.

Ea kJ mol^{-1}	**ΔH^o kJ mol^{-1}**	**ΔS^o J mol^{-1} K^{-1}**	**ΔG^o kJ mol^{-1}**
39.927	-1.524	-0.132	5.832

The decolorization of Eosin yellow dye was hastened by the increase in temperature caused by UV light, as shown in Fig.11(a,b) and Table 1. The negative $\Delta H^{\#}$, negative $\Delta S^{\#}$ and positive $\Delta G^{\#}$ indicated to the photoreaction of Eosin yellow dye decolorization are exothermic, the less random state and nonspontaneous reaction[10]. These results were considered as a good agreement with the previous published in reference [27].

Conclusions

The microwave approach was effectively used to manufacture SBA-15 mesoporous material at 100°C for 20 minutes. Tetraethyl orthosilicate (TEOS) served as the source of silica, and the structure-direction agent was the triblock polymer pluronic P123 ($EO_{20}PO_{70}EO_{20}$). The successful fabrication of a pure mesoporous material (SBA-15) was shown using characterisation methods. including XRD, TEM, BET surface, FTIR, and TGA. SBA-15 was found to have a surface area of 392.96 $m^2 \cdot g^{-1}$, a pore volume of 1.4493$cm^3 \cdot g^{-1}$, and a pore size of 9.285 cm^3/g, as determined via the BET analysis method. thermodynamic function for active case in photo reaction ($\Delta H^{\#}$, $\Delta S^{\#}$ and $\Delta G^{\#}$) were measured. Eosin yellow dye has reached the ideal concentrations for decolorization in photo-decolorization at 5 ppm, and the maximum decolorization efficiency for Eosin yellow dye is

90.71. The photo-decolorization of dispersive Eosin yellow dye was demonstrated to be a pseudo first order kinetic reaction under these investigated conditions, as the increased influence of temperature boosted the photoreaction with low values of activation energies.

Acknowledgments

The authors would like to thank the University of Kerbala, College of Science, Department of Chemistry for their support in this study, the practical part of which was undertaken in their chemistry laboratory.

REFERENCES

[1] Abbas, S.K. Hassan ZM, Mihsen HH. (2020) 'Uptake of Nickel(II) Ion by Silica-o-Phenylenediamine Derived from Rice Husk Ash', *Silicon*, 12(5), pp. 1103–1110. Available at: https://doi.org/10.1007/s12633-019-00207-4.

[2] Mihsen, H.H. and Sobh, H.S. (2018) 'Preparation and characterization of thiourea-silica hybrid as heterogeneous catalyst', *Asian Journal of Chemistry*, 30(5). Available at: https://doi.org/10.14233/ajchem.2018.20894.

[3] Azeez F, Al-Hetlani E, Arafa M. (2018) 'The effect of surface charge on photocatalytic degradation of methylene blue dye using chargeable titania nanoparticles', *Scientific reports*, 8(1), pp. 1–9.

[4] Azimov F, Markova I, Stefanova V, Sharipov K .(2012) 'Synthesis and characterization of SBA-15 and Ti-SBA-15 nanoporous materials for DME catalysts', *Journal of the University of Chemical Technology and Metallurgy*, 47(3), pp. 333–340.

[5] Cao, L., Man, T. and Kruk, M. (2009) 'Synthesis of ultra-large-pore SBA-15 silica with two-dimensional hexagonal structure using triisopropylbenzene as micelle expander', *Chemistry of Materials*, 21(6), pp. 1144–1153.

[6] Coutinho ACSLS, Quintella SA, Araujo AS. (2007) 'Thermogravimetry applied to characterization of SBA-15 nanostructured material', *Journal of thermal analysis and calorimetry*, 87(2), pp. 457–461.

[7] Erdem S, Erdem B, Öksüzoğlu RM, Çıtak A. (2015) 'Effect of calcination temperature on the structural and magnetic properties of Ni/SBA-15 nanocomposite', *Journal of Porous Materials*, 22, pp. 689–698.

[8] Farid MAA, Hassan MA, Taufiq-Yap YH. (2018) 'Kinetic and thermodynamic of heterogeneously K3PO4/AC-catalysed transesterification via pseudo-first order mechanism and Eyring-Polanyi equation', *Fuel*, 232, pp. 653–658.

[9] Lu H, Wang J, Wang T. (2017) 'Crystallization techniques in wastewater treatment: An overview of applications', *Chemosphere*, 173, pp. 474–484.

[10] Karam FF, Saeed NHM, Al Yasasri A. (2020) 'Kinetic study for reduced the toxicity of textile dyes (reactive yellow 14 dye and reactive green dye) using UV-A Light/ZnO system', *Egyptian Journal of Chemistry*, 63(8), pp. 2987–2998.

[11] Kokunešoski M, Gulicovski J, Matović B. (2010) 'Synthesis and surface characterization of ordered mesoporous silica SBA-15', *Materials Chemistry and Physics*, 124(2–3), pp. 1248–1252.

[12] Khanh Nguyen QN, Yen NT, Hau ND, Tran HL. (2020) 'Synthesis and Characterization of Mesoporous Silica SBA-15 and ZnO/SBA-15 Photocatalytic Materials from the Ash of Brickyards', *Journal of Chemistry*, 2020(1), p. 8456194.

[13] Li R, Xue T, Li Z, Wang Q. (2020) 'Hierarchical structure ZSM-5/SBA-15 composite with improved hydrophobicity for adsorption-desorption behavior of toluene', *Chemical Engineering Journal*, 392, p. 124861.

[14] Melosh, N.A., Davidson, P. and Chmelka, B.F. (2000) 'Monolithic mesophase silica with large ordering domains', *Journal of the American Chemical Society*, 122(5), pp. 823–829.

[15] Zhao D, Feng J, Huo Q. (1998) 'Triblock copolymer syntheses of mesoporous silica with periodic 50 to 300 angstrom pores', *science*, 279(5350), pp. 548–552.

[16] Zhai Q-Z, Dong Y, Liu H, Wang Q-S. (2019) 'Adsorption of Methylene Blue onto nano SBA-15 mesoporous material from aqueous media: kinetics, isotherms and thermodynamic studies', *Desalination and Water Treatment*, 158, pp. 330–342.

[17] Kruk M, Jaroniec M, Ko CH, Ryoo R. (2000) 'Characterization of the porous structure of SBA-15', *Chemistry of materials*, 12(7), pp. 1961–1968.

[18] Zamri MFMA, Hassan SHA, Tiong SK. (2024) 'Progress and challenges of mesoporous catalysts in upgraded pyrolysis of biomass for biofuel production', *Journal of Analytical and Applied Pyrolysis*, p. 106651.

[19] Shah, P. and Ramaswamy, V. (2008) 'Thermal stability of Mesoporous SBA-15 and Sn-SBA-15 Molecular Sieves: An in situ HTXRD study', *Microporous and Mesoporous*

Materials, 114(1–3), pp. 270–280.

[20] Yeh, Y.-Q., Tang, C.-Y. and Mou, C.-Y. (2014) 'Two-dimensional crystals of mesoporous silica SBA-15 nanosheets with perpendicular and open channels', *APL Materials*, 2(11).

[21] Ollis, D., Silva, C.G. and Faria, J. (2015) 'Simultaneous photochemical and photocatalyzed liquid phase reactions: Dye decolorization kinetics', *Catalysis Today*, 240, pp. 80–85.

[22] Ahmed, L.M. (2018) 'Photo-decolourization kinetics of acid red 87 dye in ZnO suspension under different types of UV-A light', *Asian J. Chem*, 30(9), pp. 2134–2140.

[23] Ridha NJ, Alosfur FKM, Kadhim HBA, Ahmed LM. (2021) 'Synthesis of Ag decorated TiO_2 nanoneedles for photocatalytic degradation of methylene blue dye', *Materials Research Express*, 8(12), p. 125013.

[24] Yang J, Zhang J, Zhu L. (2006) 'Synthesis of nano titania particles embedded in mesoporous SBA-15: characterization and photocatalytic activity', *Journal of Hazardous Materials*, 137(2), pp. 952–958.

[25] Nasiri A, Tamaddon F, Mosslemin MH. (2019) 'Magnetic nano-biocomposite CuFe2O4@ methylcellulose (MC) prepared as a new nano-photocatalyst for degradation of ciprofloxacin from aqueous solution', *Environmental health engineering and management journal*, 6(1), pp. 41–51.

[26] Kumar, D.J.V. (2016) *Determination of activation energy for encapsulant browning of photovoltaic modules*. Arizona State University.

[27] Pitre, S.P., McTiernan, C.D. and Scaiano, J.C. (2016) 'Understanding the kinetics and spectroscopy of photoredox catalysis and transition-metal-free alternatives', *Accounts of Chemical Research*, 49(6), pp. 1320–1330.